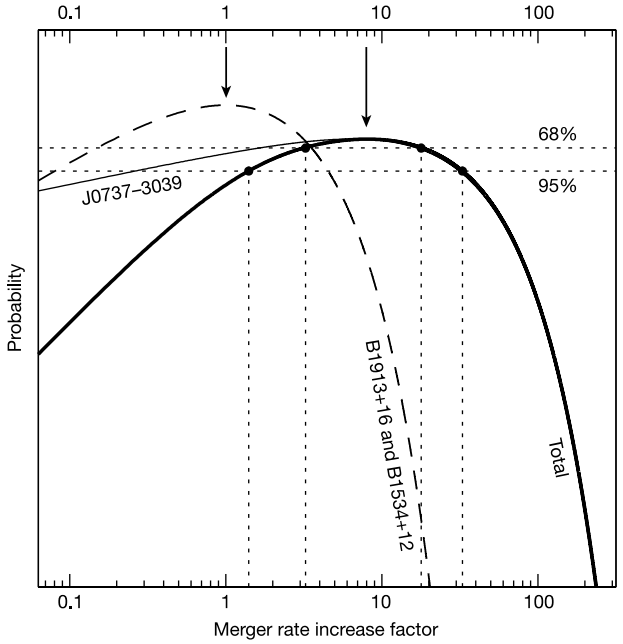

Figure 2 Probability density function for the increase in the double-neutron-star merger rate $(R_{0737}+R_{1913}+R_{1534})/(R_{1913}+R_{1534})$ resulting from the discovery of PSR J0737–3039. For a given class k of binary pulsars in the Galaxy, the probability density function $P(R_k)$ for the corresponding merger rate R_k is obtained from the relation[6] $P(R_k)=A^2R_k e^{-AR_k}$ where $A=\tau_k/(N_k f_k)$, N_k is a population scaling factor (see text), τ_k is the binary pulsar lifetime and f_k is the correction factor due to the beamed nature of the radio pulsar emission. The dashed line represents the reference probability density function corresponding to the merger rate $R_{old}=R_{1913}+R_{1534}$ due to PSR B1913+16 and PSR B1534+12 only[6]. The heavy solid line represents the probability density function corresponding to the new merger rate $R_{new}=R_{0737}+R_{1913}+R_{1534}$. The parameters adopted for PSR J0737–3039 are those derived in the text ($N_{0737}=6N_{1913}$, $\tau_{0737}=185$ Myr) and the beaming factor for PSR J0737–3039, f_{0737}, is chosen as the average of the beaming factor of the other two known merging binaries ($f_{0737}=1.06f_{1913}$). The dotted vertical lines represent the 68% and 95% confidence level boundaries on the determination of the increase factor. The dominant role of PSR J0737–3039 in shaping the new statistics of the double-neutron-star merger rate is evident.

Extensive simulations (V.K. *et al.*, manuscript in preparation) produce results consistent with that derived in Fig. 2, and show that the peak of the merger rate increase factor resulting from the discovery of PSR J0737–3039 lies in the range 6 to 7 and is largely independent of the adopted pulsar population model. On the other hand, the actual predicted value of the Galactic merger rate and hence the detection rate by gravity wave detectors depends on the shape of the pulsar luminosity function. For the most favourable distribution model available (model 15 of ref. 6), the updated cosmic detection rate for first-generation gravity wave detectors such as VIRGO[24], LIGO[25] and GEO[26] can be as high as 1 every 1–2 yr at the 95% confidence level.

After a few years of operation of the gravity wave detectors, it should be possible to test these predictions directly and thus place better constraints on the cosmic population of double-neutron-star binaries. □

Received 12 August; accepted 15 October 2003; doi:10.1038/nature02124.

1. Misner, C., Thorne, K. S. & Wheeler, J. A. *Gravitation* Ch. 36 (Freeman, New York, 1973).
2. Schutz, B. GW, sources, and physics overview: Proc. 5th Edoardo Amaldi Conf. on Gravitational Waves. *Class. Quant. Grav.* (special issue) (in the press).
3. Curran, S. J. & Lorimer, D. R. Pulsar statistics. Part 3: Neutron star binaries. *Mon. Not. R. Astron. Soc.* **276,** 347–352 (1995).
4. Arzoumanian, Z., Cordes, J. M. & Wasserman, I. Pulsar spin evolution, kinematics, and the birthrate of neutron star binaries. *Astrophys. J.* **520,** 696–705 (1999).
5. Kalogera, V., Narayan, R., Spergel, D. N. & Taylor, J. H. The coalescence rate of double neutron star systems. *Astrophys. J.* **556,** 340–356 (2001).
6. Kim, C., Kalogera, V. & Lorimer, D. R. The probability distribution of binary pulsar coalescence rates. I. Double neutron star systems in the galactic field. *Astrophys. J.* **584,** 985–995 (2003).
7. van den Heuvel, E. P. J. & Lorimer, D. R. On the Galactic and cosmic merger rate of double neutron stars. *Mon. Not. R. Astron. Soc.* **283,** L37–L39 (1996).
8. Staveley-Smith, L. *et al.* The Parkes 21 cm multibeam receiver. *Publ. Astron. Soc. Aust.* **13,** 243–248 (1996).
9. Taylor, J. H., Fowler, L. A. & McCulloch, P. M. Measurements of general relativistic effects in the binary pulsar PSR 1913+16. *Nature* **277,** 437–440 (1979).
10. Thorsett, S. E. & Chakrabarty, D. Neutron star mass measurements. I. Radio pulsars. *Astrophys. J.* **512,** 288–299 (1999).
11. Srinivasan, G. & van den Heuvel, E. P. J. Some constraints on the evolutionary history of the binary pulsar PSR 1913+16. *Astron. Astrophys.* **108,** 143–147 (1982).
12. Roberts, D. H., Masters, A. R. & Arnett, W. D. Determining the stellar masses in the binary system containing the pulsar PSR 1913+16—Is the companion a helium main-sequence star? *Astrophys. J.* **203,** 196–201 (1976).
13. Smarr, L. L. & Blandford, R. The binary pulsar—Physical processes, possible companions, and evolutionary histories. *Astrophys. J.* **207,** 574–588 (1976).
14. Wex, N. A timing formula for main-sequence star binary pulsars. *Mon. Not. R. Astron. Soc.* **298,** 66–77 (1998).
15. Weisberg, J. M. & Taylor, J. H. General relativistic geodetic spin precession in binary pulsar B1913+16: Mapping the emission beam in two dimensions. *Astrophys. J.* **576,** 942–949 (2002).
16. Damour, T. & Taylor, J. H. On the orbital period change of the binary pulsar PSR 1913+16. *Astrophys. J.* **366,** 501–511 (1991).
17. Taylor, J. H. Binary pulsars and relativistic gravity. *Rev. Mod. Phys.* **66,** 711–719 (1994).
18. Shapiro, I. I. Fourth test of general relativity. *Phys. Rev. Lett.* **13,** 789–791 (1964).
19. Peters, P. C. & Mathews, J. Gravitational radiation from point masses in a keplerian orbit. *Phys. Rev.* **131,** 435–440 (1963).
20. Taylor, J. H. Pulsar timing and relativistic gravity. *Phil. Trans. R. Soc. Lond.* **341,** 117–134 (1992).
21. Phinney, E. S. The rate of neutron star binary mergers in the universe—Minimal predictions for gravity wave detectors. *Astrophys. J.* **380,** L17–L21 (1991).
22. Taylor, J. H. & Cordes, J. M. Pulsar distances and the galactic distribution of free electrons. *Astrophys. J.* **411,** 674–684 (1993).
23. Manchester, R. N. *et al.* The Parkes multi-beam pulsar survey—I. Observing and data analysis systems, discovery and timing of 100 pulsars. *Mon. Not. R. Astron. Soc* **328,** 17–35 (2001).
24. Bradaschia, C., *et al.* in *Gravitational Astronomy: Instrument Design and Astrophysical Prospects* (eds McClelland, D. E. & Bachor, H. A.) 110–115 (Elizabeth and Frederick White Research Conference Proceedings, World Scientific, Singapore, 1991).
25. Abramovici, A. *et al.* LIGO—The Laser Interferometer Gravitational-Wave Observatory. *Science* **256,** 325–333 (1992).
26. Danzmann, K., *et al.* in *First Edoardo Amaldi Conf. on Gravitational Wave Experiments* (eds Coccia, E., Pizzella, G. & Ronga, F.) 100–111 (World Scientific, Singapore, 1995).
27. Damour, T. & Deruelle, N. General relativistic celestial mechanics of binary systems. II. The post-Newtonian timing formula. *Ann. Inst. H. Poincaré (Phis. Théor.)* **44,** 263–292 (1986).
28. Manchester, R. N. & Taylor, J. H. *Pulsars* Ch. 9 (Freeman, San Francisco, 1977).

Acknowledgements We thank J. Reynolds of the Parkes Observatory, and B. Sault of the ATCA, for prompt allocations of observing time. The Parkes Observatory and the ATCA are part of the Australia Telescope, which is funded by the Commonwealth of Australia for operation as a National Facility managed by CSIRO. M.B., N. D'A. and A.P. acknowledge financial support from the Italian Ministry of University and Research (MIUR) under the national programme 'Cofin 2001'. V.K. acknowledges partial support by a David and Lucile Packard Science and Engineering Fellowship and a NSF Gravitational Physics grant. D.R.L. is a University Research fellow funded by the Royal Society.

Competing interests statement The authors declare that they have no competing financial interests.

Correspondence and requests for materials should be addressed to N. D'A. (damico@ca.astro.it).

Continuous magnetic reconnection at Earth's magnetopause

H. U. Frey[1], T. D. Phan[1], S. A. Fuselier[2] & S. B. Mende[1]

[1]*Space Sciences Laboratory, University of California, Berkeley, California 94720-7450, USA*
[2]*Lockheed Martin Advanced Technology Center, Palo Alto, California 94304, USA*

The most important process that allows solar-wind plasma to cross the magnetopause and enter Earth's magnetosphere is the merging between solar-wind and terrestrial magnetic fields of opposite sense—magnetic reconnection[1]. It is at present not known whether reconnection can happen in a continuous fashion or whether it is always intermittent. Solar flares[2] and magneto-

spheric substorms[3]—two phenomena believed to be initiated by reconnection—are highly burst-like occurrences, raising the possibility that the reconnection process is intrinsically intermittent, storing and releasing magnetic energy in an explosive and uncontrolled manner. Here we show that reconnection at Earth's high-latitude magnetopause is driven directly by the solar wind, and can be continuous and even quasi-steady over an extended period of time. The dayside proton auroral spot in the ionosphere—the remote signature of high-latitude magnetopause reconnection[4]—is present continuously for many hours. We infer that reconnection is not intrinsically intermittent; its steadiness depends on the way that the process is driven.

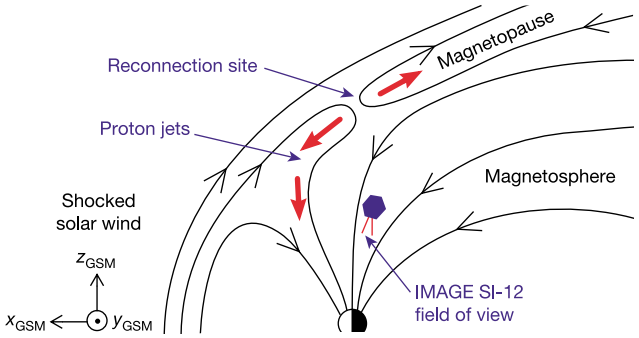

Figure 1 Diagram showing the link between reconnection at the magnetopause and its footprint in the ionosphere. The dayside proton auroral spot imaged by the IMAGE spacecraft (see Fig. 2) is created by precipitating solar wind protons that have crossed the high-latitude magnetopause and were accelerated by the magnetic kink resulting from magnetic reconnection between the solar-wind's and Earth's magnetic fields. Reconnection in this case happens between a northward (up in the figure) along the *z* axis of the geocentric solar magnetospheric (GSM) coordinate system directed solar-wind magnetic field and opposite magnetospheric field lines at the high-latitude location.

Models of reconnection are typically steady state. They describe what happens once the process is initiated and allowed to proceed indefinitely. Transient reconnection models have also been developed, which describe the consequence of artificially varying the reconnection rate, even including times when the rate drops to zero[5]. A key unanswered question, both theoretically and observationally, is how long the process can maintain itself naturally once initiated[6]. In other words, is the process intrinsically intermittent or continuous? Intermittent reconnection turns on and off. Continuous reconnection operates at a variable rate but never ceases; if the fluctuation is a small fraction of the average then the reconnection is classed as 'quasi-steady'. Attempts to deduce the steadiness of reconnection on the basis of *in situ* magnetopause observations were inconclusive[7]. Because signatures of reconnection (for example, plasma jets) are localized in the thin magnetopause, they can be observed only for a short time (a few minutes) when a spacecraft intersects the layer, even if the reconnection is actually continuous. Much of the published literature from ground-based or *in situ* measurements in the cusp has reported intermittent reconnection[8–12].

It has been established recently that the dayside proton auroral spot[13,14] is created directly by solar-wind protons leaking through, and accelerated at, the magnetopause by way of reconnection between solar-wind and magnetospheric magnetic fields[4] (Fig. 1). The proton aurora spot is detected by the SI-12 imager on the IMAGE spacecraft[15]. It detects the Doppler-shifted Lyman-α photons corresponding to precipitating charge-exchanged protons with energies of a few keV. As this is not the average energy of a typical proton distribution in the shocked solar wind, some sort of energization process is required. Magnetic reconnection at the magnetopause readily provides this energization[4]. Thus, the SI-12 imager is well suited to provide global images of the aurora created from precipitating protons that have been energized by magnetic reconnection at an active reconnection site.

Here we report two notable examples of long-duration proton auroral spot observations that imply continuous and even quasi-

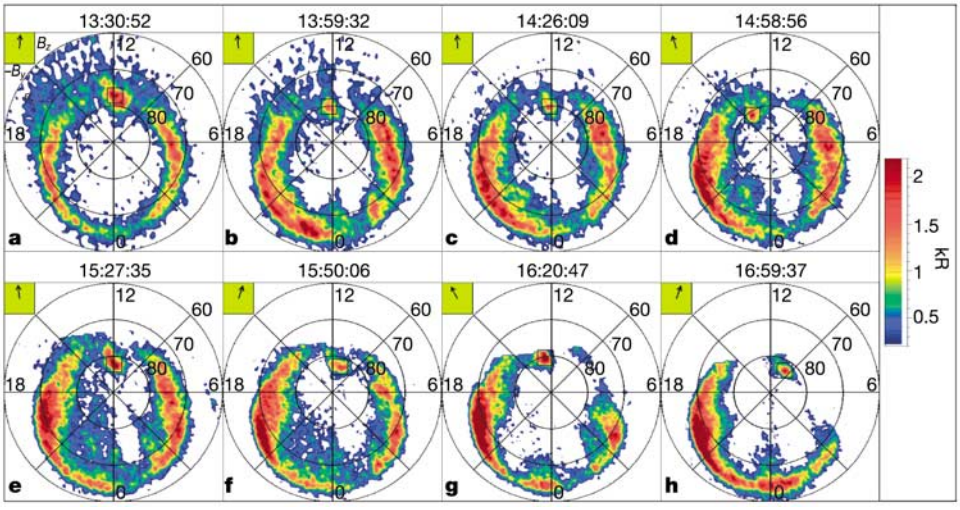

Figure 2 Snapshots of the proton aurora oval and spot on 18 March 2002 showing the continuous presence of the proton aurora spot. The Spectrographic Imager channel SI-12 on board the IMAGE spacecraft observes precipitating, high-energy protons[15]. On their way down along magnetic field lines, energetic protons temporarily capture electrons from the high-altitude atmospheric atoms and molecules. These newly formed hydrogen atoms may be in an excited state. When the atom decays to the ground state it releases a photon at the Lyman-α wavelength (121.567 nm). The SI-12 observes Doppler-shifted Lyman-α emission from precipitating protons with energy of several keV. The images are shown in a geomagnetic grid of latitudes and local time with the noon meridian at the top and morning 06:00 h pointing to the right. The solar-wind magnetic field in y_{GSM}–z_{GSM} plane is shown in the upper left inset, with north ($B_z > 0$) pointing up and east ($B_y > 0$) pointing to the left. The black square in each panel covers the 500 × 500 km^2 area around the spot used in the computation of the mean brightness in Fig. 3c. The dayside proton aurora spot is seen uninterruptedly over ~4 h. The spot appears on the dayside at ~80° latitude. Its location in magnetic local time (MLT) is correlated with the *y*-component of the solar-wind magnetic field, being in the pre-noon (post-noon) sector for negative (positive) B_y. Colour scale shows Lyman-α brightness in kilorayleighs, kR.

steady magnetopause reconnection for many hours. These observations were made during northward solar-wind magnetic field conditions, when the reconnection site is expected to be at the high-latitude magnetopause where the solar-wind and magnetospheric magnetic fields are antiparallel (Fig. 1).

The first reconnection event occurred on 18 March 2002 (Fig. 2). For the entire ~4-h interval shown, the solar-wind dynamic pressure (Fig. 3a) was constant (~17 nPa). The solar-wind magnetic field (B, Fig. 3b) was persistently northward directed ($B_z > 0$) while its y (east–west) component (B_y) fluctuated between positive and negative. Figures 2 and 3c–e show the uninterrupted presence of a bright proton auroral spot during this ~4-h interval. During a brief interval (5 min), the Cluster spacecraft by chance crossed the high-latitude magnetopause and observed proton jets accelerated by reconnection at the magnetopause[4]. The reconnection jets were observed on field lines that are linked to the spot in the ionosphere and with energy fluxes consistent with the spot brightness, thus providing direct evidence that the spot represents the remote signature of high-latitude magnetopause reconnection. Although Cluster could only observe reconnection for 5 min, the uninterrupted presence of the spot in the images in Fig. 2 implies continuous reconnection over ~4 h. Note that the peak and average brightness of the spot (Fig. 3c) remained high over the whole observation period, with some fluctuations.

After 14:40 UT, the magnetic local time (MLT) location of the spot (Figs 2, 3e) follows very closely the changes in the y component of the solar-wind magnetic field (Fig. 3b), with spot locations at pre-noon MLT for negative B_y and with post-noon locations with positive B_y (ref. 16). The correlation implies that reconnection is a directly driven process at the magnetopause and is consistent with antiparallel reconnection. That is, the reconnection site is located where the internal magnetospheric magnetic field is antiparallel to the external shocked solar-wind field[14,17]. As the solar-wind magnetic field changes, the antiparallel reconnection site moves on the magnetopause. This is seen in the ionosphere as motion in MLT but not in latitude. This motion, combined with the near-constant brightness of the spot, indicates that the reconnection site is continuously active (not intermittent). Thus, viewed globally, the reconnection process never stops at the high-latitude magnetopause. Finally, as the spot moves in MLT in response to the solar wind B_y, it does not leave a long trail in latitude or in MLT, which would have indicated that proton aurorae are still created long (more than 4–5 min) after the cessation of reconnection.

The second continuous reconnection event occurred on 17/18 September 2000 (Fig. 4). This event does not have the added benefit of simultaneous *in situ* observations at the magnetopause. However, it is remarkable in that the dayside proton aurora spot was observed uninterruptedly for ~9 h (01:00–10:00 on 18 September), in addition to more than 3 h of continuous presence of the bright proton spot during the previous IMAGE apogee (northern hemisphere) pass (16:20–19:30 UT on 17 September). Before 05:45 UT on 18 September, similar to the previous event, the MLT location of the spot is well correlated with changes in the y-component of the solar-wind magnetic field, with similar implications in terms of antiparallel reconnection. Between 05:45 and 09:00 UT on 18 September, however, the solar-wind pressure and magnetic field direction were nearly constant. The proton spot brightness and location during the corresponding interval were also remarkably stable. Furthermore, the poleward boundary of the proton aurora spot (red line in Fig. 4d) was also rather stable. This stability rules out bursts of reconnection with periods longer than 4–5 min (the images are obtained on a two-minute cadence). Longer periods of reconnection bursts would produce observable brightness and size changes, slow periodic equatorward motions, and sudden poleward jumps of the proton spot poleward boundary.

The above observations can be summarized and further interpreted as follows. The dayside proton auroral spot, which recently has been shown to be the footprint of high-latitude reconnection, was observed continuously for close to 4 h in one event and more than 9 h in another. The continuous presence of the spot even as the solar-wind condition changed implies that continuous magnetic reconnection was occurring over these time spans. In a global sense, it is significant that reconnection at the high-latitude magnetopause never stops for any period of time longer than 4-5 min. For more stable solar-wind conditions in the second half of the second event, reconnection is continuous not only in a global sense, but its rate appears quasi-steady at the local magnetopause as well. The present finding explains the persistence of optical signatures of the cusp from ground-based observations during stable solar-wind magnetic field conditions[18–20].

For low-latitude reconnection during southward solar-wind magnetic field conditions, it was reported that the proton aurora could be seen on each reconnected field line for up to 5 min following reconnection[21]. In the present high-latitude reconnection case, this time might be longer. Any intermittency in the reconnection rate on 5 min or longer timescales should create observable signatures (changes in spot brightness and latitude) in the proton

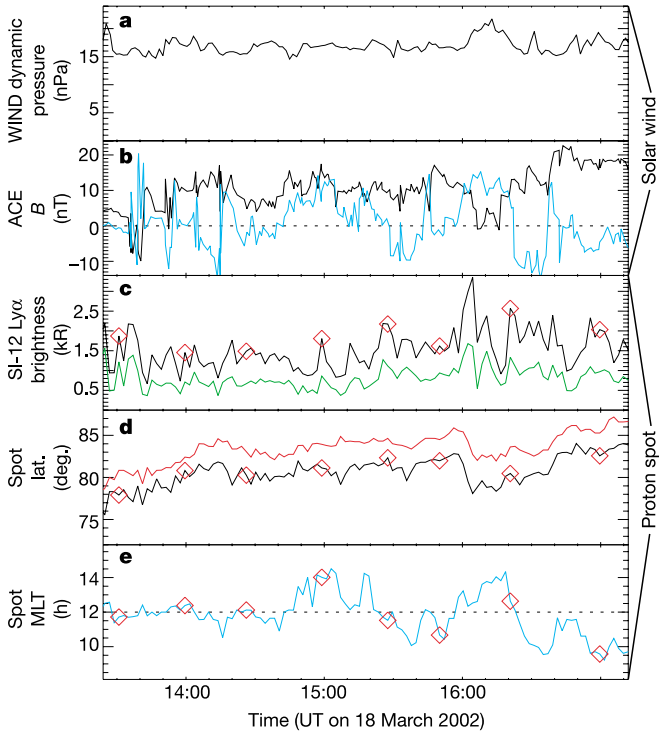

Figure 3 Continuous presence of dayside proton aurora spot (and implied reconnection) for ~4 h on 18 March 2002. **a**, The solar-wind dynamic pressure—measured by the WIND spacecraft and shifted in time by an average of 7 min to take into account the solar-wind convection time from the WIND position to the high-latitude magnetopause—was constant (~17 nPa) throughout this interval. **b**, The y (blue) and z (black) components of the solar-wind magnetic field measured by the ACE spacecraft, shifted in time by an average of 58 min. The field was mostly directed northward during the entire interval while the y-component is variable. **c**, IMAGE SI-12 detected peak (black) and mean (green) (averaged over 500 × 500 km^2 area around the brightest pixel) Lyman-α brightness of the dayside proton auroral spot. Times of image snapshots shown in Fig. 2 are marked with red diamonds. **d**, **e**, The locations of the proton spot in magnetic latitude (black line in **d**) and MLT (blue line in **e**). In **d** we also show the location of the poleward boundary of the proton aurora spot (red line). Note the remarkable correlation between the spot MLT and the east–west (y) component of the solar-wind magnetic field (blue line in **b**) after 14:40 UT.

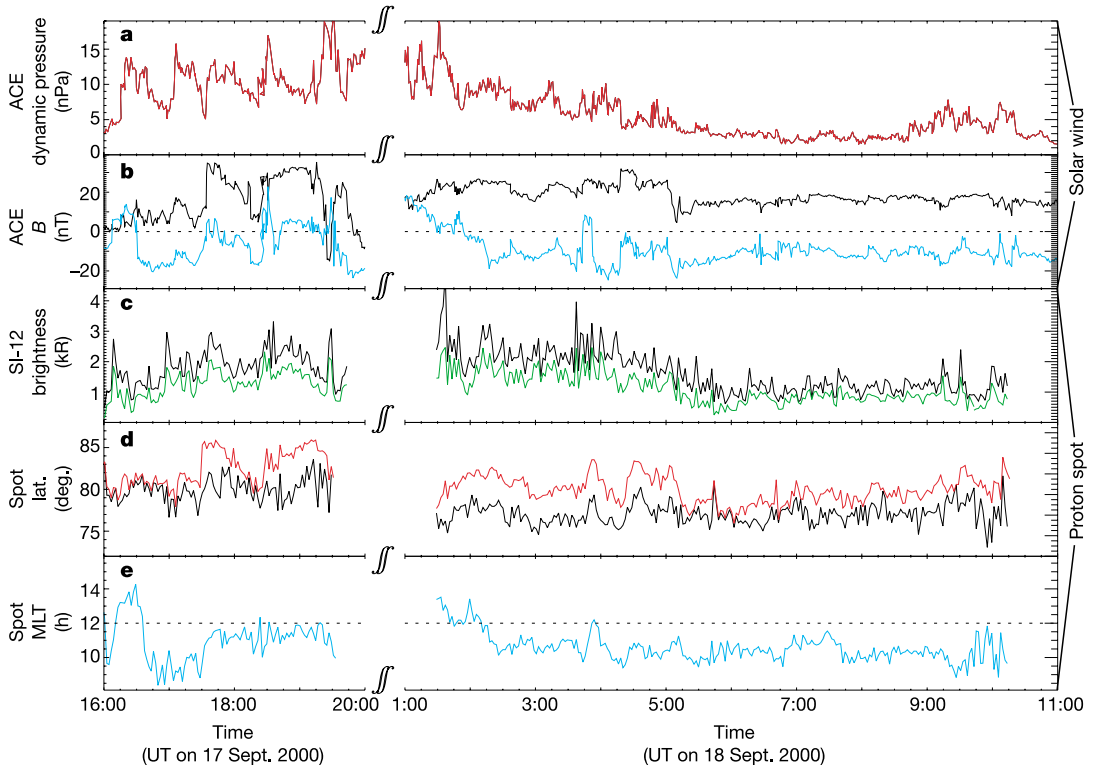

Figure 4 Continuous presence of dayside proton aurora spot (and implied reconnection) for ~9 h on 17/18 September 2000. The parameters are similar to Fig. 2. Note the remarkable steadiness of the spot brightness and location in magnetic latitude (**d**) and local time (**e**) from 05:45 to 09:00 UT on 18 September during steady solar-wind pressure (**a**) and magnetic field (**b**) conditions. At other times, the spot location is correlated with the east–west (y) component of the solar-wind magnetic field, and its brightness is correlated with the solar-wind pressure. Between 19:30 and 01:20 UT there were no proton aurora observations by IMAGE because the spacecraft moved through perigee in the southern hemisphere.

aurora image sequences. Such changes are not seen in our 2-min-resolution images. Thus our findings are in contrast to reports favouring intermittent reconnection, which were made mostly under southward solar-wind magnetic field conditions[8–10,12]. This contrast is more surprising considering that reconnection is thought to be more intermittent during northward solar-wind magnetic field, when the reconnection site is located at the high-latitude magnetopause (as opposed to a low-latitude site for southward solar-wind magnetic field) owing to the presence of fast shocked solar-wind flows[22]. A possible explanation for this discrepancy is the fact that most of the previous studies of reconnection have been made locally using ground-based or *in situ* measurements, which could not distinguish temporal variations of reconnection from motion of the reconnection site if the solar-wind magnetic field is not steady. At the local magnetopause, reconnection could well be intermittent if the solar-wind field changes.

The present results suggest that reconnection for northward solar-wind magnetic field is a directly driven process that is continuous when viewed in a global sense, or even in a local sense when the solar-wind conditions are steady. This regime of reconnection is in stark contrast to the storage and release of magnetic energy in explosive reconnection at the Sun (associated with solar flares) or in the magnetotail (associated with magnetospheric substorms). This contrast may suggest that, if driven persistently—in this case the shocked solar wind impinges on the magnetopause continuously—the process can be continuous. To evaluate fully the controlling factors that dictate the temporal behaviour of reconnection is a major objective of the planned NASA Magnetospheric Multiscale mission[6]. □

Received 13 June; accepted 23 September 2003; doi:10.1038/nature02084.

1. Cowley, S. W. H. in *Magnetic Reconnection in Space and Laboratory Plasmas* (ed. Hones, E. W.) 375–378 (Geophysics Monograph 30, American Geophysical Union, Washington DC, 1984).
2. Hudson, H. & Ryan, J. High-energy particles in solar flares. *Annu. Rev. Astron. Astrophys.* **33,** 239–282 (1995).
3. Angelopoulos, V. *et al.* Statistical characteristics of bursty bulk flow events. *J. Geophys. Res.* **103,** 21257–21280 (1994).
4. Phan, T. *et al.* Simultaneous Cluster and IMAGE observations of cusp reconnection and auroral proton spot for northward IMF. *Geophys. Res. Lett.* **30,** doi:10.1029/2003GL016885 (2003).
5. Scholer, M. Magnetic flux transfer at the magnetopause based on single X line bursty reconnection. *Geophys. Res. Lett.* **15,** 291–294 (1988).
6. *Report of the NASA Science and Technology Definition Team for the Magnetospheric Multiscale (MMS) Mission* (NASA/TM-2000–209883, Goddard Space Flight Center, Greenbelt, MD, 1999).
7. Phan, T. D. *et al.* Extended magnetic reconnection at the Earth's magnetopause from detection of bi-directional jets. *Nature* **404,** 848–850 (2000).
8. Farrugia, C. J., Sandholt, P. E., Denig, W. F. & Torbert, R. B. Observation of a correspondence between poleward moving auroral forms and stepped cusp ion precipitation. *J. Geophys. Res.* **103,** 9309–9315 (1998).
9. Lockwood, M. *et al.* Cusp ion steps, field-aligned currents and poleward moving auroral forms. *J. Geophys. Res.* **106,** 29555–29569 (2001).
10. Lockwood, M., Davis, C. J., Onsager, T. G. & Scudder, J. D. Modelling signatures of pulsed magnetopause reconnection in cusp ion dispersion signatures seen at middle altitudes. *Geophys. Res. Lett.* **25,** 591–594 (1998).
11. Sandholt, P. E. *et al.* Dynamic cusp aurora and associated pulsed reverse convection during northward interplanetary magnetic field. *J. Geophys. Res.* **105,** 12869–12894 (2000).
12. Milan, S. E., Lester, M., Greenwald, R. A. & Sofko, G. The ionospheric signature of transient dayside reconnection and the associated pulsed convection return flow. *Ann. Geophys.* **17,** 1166–1171 (1999).
13. Frey, H. U. *et al.* Proton aurora in the cusp. *J. Geophys. Res. A* **107,** doi:10.1029/2001JA900161 (2002).
14. Fuselier, S. A. *et al.* Cusp aurora dependence on IMF B_z. *J. Geophys. Res. A* **107,** doi:10.1029/2001JA900165 (2002).
15. Mende, S. B. *et al.* Far ultraviolet imaging from the IMAGE spacecraft: 3. Spectral imaging of Lyman alpha and OI 135.6 nm. *Space Sci. Rev.* **91,** 287–318 (2000).
16. Newell, P. T., Meng, C.-I., Sibeck, D. G. & Lepping, R. Some low-altitude cusp dependencies on the interplanetary magnetic field. *J. Geophys. Res.* **94,** 8921–8927 (1989).
17. Frey, H. U., Mende, S. B., Fuselier, S. A., Immel, T. J. & Ostgaard, N. Proton aurora in the cusp during southward IMF. *J. Geophys. Res. A* **108,** doi:10.1029/2003JA009861 (2003).
18. Mende, S. B., Rairden, R. L., Lanzerotti, L. J. & Maclennan, C. G. Magnetic impulses and associated optical signatures in the dayside aurora. *Geophys. Res. Lett.* **17,** 131–134 (1990).

19. Sandholt, P. E. IMF control of polar cusp and cleft auroras. *Adv. Space Res.* **8,** 21–34 (1988).
20. Newell, P. T. Do the dayside cusps blink? *Rev. Geophys. Suppl.* **33,** 665–668 (1995).
21. Lockwood, M. *et al.* IMF control of cusp proton emission intensity and dayside convection: Implications for component and anti-parallel reconnection. *Ann. Geophys.* **21,** 955–982 (2003).
22. Cowley, S. W. H. & Owen, C. J. A simple illustrative model of open flux tube motion over the dayside magnetopause. *Planet. Space Sci.* **37,** 1461–1475 (1989).

Acknowledgements We are indebted to the IMAGE team and J. L. Burch for the design and successful operation of the IMAGE mission.

Competing interests statement The authors declare that they have no competing financial interests.

Correspondence and requests for materials should be addressed to H.U.F. (hfrey@ssl.berkeley.edu).

Emergence of a molecular Bose–Einstein condensate from a Fermi gas

Markus Greiner[1], Cindy A. Regal[1] & Deborah S. Jin[2]

[1]*JILA, National Institute of Standards and Technology and Department of Physics, University of Colorado,* [2]*Quantum Physics Division, National Institute of Standards and Technology, Boulder, Colorado 80309-0440, USA*

The realization of superfluidity in a dilute gas of fermionic atoms, analogous to superconductivity in metals, represents a long-standing goal of ultracold gas research. In such a fermionic superfluid, it should be possible to adjust the interaction strength and tune the system continuously between two limits: a Bardeen–Cooper–Schrieffer (BCS)-type superfluid (involving correlated atom pairs in momentum space) and a Bose–Einstein condensate (BEC), in which spatially local pairs of atoms are bound together. This crossover between BCS-type superfluidity and the BEC limit has long been of theoretical interest, motivated in part by the discovery of high-temperature superconductors[1–10]. In atomic Fermi gas experiments superfluidity has not yet been demonstrated; however, long-lived molecules consisting of locally paired fermions have been reversibly created[11–15]. Here we report the direct observation of a molecular Bose–Einstein condensate created solely by adjusting the interaction strength in an ultracold Fermi gas of atoms. This state of matter represents one extreme of the predicted BCS–BEC continuum.

The basic idea behind this experiment is to start with a Fermi gas that has been evaporatively cooled to a high degree of quantum degeneracy, and adiabatically create molecules with a magnetic-field sweep across a Feshbach resonance. If the molecule creation conserves entropy and the initial atom gas is at sufficiently low temperature T compared to the Fermi temperature T_F, then the result should be a molecular sample with a significant condensate fraction[13,16]. With a relatively slow sweep of an applied magnetic field that converts most of the fermionic atoms into bosonic molecules and an initial atomic gas below $T/T_F = 0.17$, we observe a molecular condensate in time-of-flight absorption images taken immediately following the magnetic-field sweep. The molecular condensate is not formed by any active cooling of the molecules, but rather merely by traversing the predicted BCS–BEC crossover regime.

Our experimental set-up and the procedure used to cool a gas of fermionic ^{40}K atoms to quantum degenerate temperatures have been detailed in previous work[17,18]. In brief, after laser cooling and trapping we evaporatively cool the atoms in a magnetic trap. In order to realize *s*-wave collisions in the ultracold Fermi gas, we use a mixture of atoms in two different spin states. For the final stage of evaporative cooling, the atoms are loaded into an optical dipole trap formed by a single far-red-detuned laser beam. The laser wavelength is $\lambda = 1{,}064$ nm, and the beam is focused to a waist of 15.5 μm. By lowering the depth of the optical trap, we evaporate the atomic gas to temperatures far below the Fermi temperature $T_F = (6N\nu_r^2\nu_z)^{1/3}h/k_B$. Here N is the particle number in each spin state, ν_r and ν_z are the radial and axial trap frequencies, h is Planck's constant, and k_B is Boltzmann's constant. For final radial trap frequencies between $\nu_r = 430$ Hz and 250 Hz and a fixed trap aspect ratio $\nu_r/\nu_z = 79 \pm 15$, we achieve temperatures between $0.36T_F$ and $0.04T_F$. (All temperatures of the Fermi gas given in this work are determined through surface fits to time-of-flight absorption images[18].)

For this work we use a Feshbach resonance, which occurs when the energy of a quasibound molecular state becomes equal to the energy of two free atoms. The magnetic-field dependence of the resonance allows precise tuning of the atom–atom interaction strength in an ultracold gas[19]. Moreover, time-dependent magnetic fields can be used to reversibly convert atom pairs into extremely weakly bound molecules[11–14,20–24]. The particular resonance used here is located at a magnetic field $B_0 = 202.1 \pm 0.1$ G and has a width of $w = 7.8 \pm 0.6$ G (refs 15, 25). The resonance affects collisions between atoms in the two lowest-energy spin states $|f = 9/2, m_f = -7/2\rangle$ and $|f = 9/2, m_f = -9/2\rangle$ of ^{40}K, where f denotes the total atomic angular momentum and m_f the magnetic quantum number.

To create bosonic molecules from the fermionic atoms, we first prepare an equal mixture of atoms in the $m_f = -9/2$ and $m_f = -7/2$ spin states at temperatures below quantum degeneracy. Then we apply a time-dependent sweep of the magnetic field starting above the Feshbach resonance value, where the atom interactions are effectively attractive, and ending below the resonance, where the atom interactions are effectively repulsive. In contrast to our previous work[11], the magnetic-field sweep is not only adiabatic with respect to the molecule creation rate, but also slow with respect to the collision rate and the radial trap frequency[13]. The magnetic field is typically ramped in 7 ms from $B = 202.78$ G to either $B = 201.54$ G or $B = 201.67$ G. With this magnetic-field sweep across the Feshbach resonance we convert between 78% and 88% of the atoms into molecules. To a very good approximation, these molecules have twice the polarizability of the atoms[26] and therefore are confined in the optical dipole trap with the same trapping frequency and twice the trap depth of the atoms. The molecules, which are all in the same internal quantum state, are highly vibrationally excited, very large in spatial extent, and extremely weakly bound. For a magnetic field 0.43 G below the Feshbach resonance ($B = 201.67$ G) the binding energy $\hbar^2/ma^2$ is 8 kHz, where m is the atomic mass and $2\pi\hbar$ is Planck's constant. The molecule size, which we estimate as $a/2$, is $\sim 1{,}650a_0$, where a_0 is the Bohr radius and a is the atom–atom scattering length given by $a = 174a_0[1 + w/(B_0 - B)]$ (ref. 18). At this magnetic field, the molecule size is one order of magnitude smaller than the calculated intermolecular distance.

A critical element of this experiment is that the lifetime of these weakly bound molecules can be much longer than the typical collision time in the gas and longer than the radial trapping period[12–15]. In previous work, we found that the $^{40}K_2$ molecule lifetime increases dramatically near the Feshbach resonance and reaches ~100 ms at a magnetic field 0.43 G below the Feshbach resonance for a peak density of $n_{pk} = 1.5 \times 10^{13}$ cm^{-3} (ref. 15). It is predicted that this increased molecule lifetime only occurs for dimers of fermionic atoms[27]. The relatively long molecule lifetime near the Feshbach resonance allows the atom/molecule mixture to achieve thermal equilibrium during the magnetic-field sweep. Note, however, that the large aspect ratio of the optical trap gives rise to a